JACS
JOURNAL OF THE AMERICAN CHEMICAL SOCIETY

Article

pubs.acs.org/JACS

Growth of Thin, Anisotropic, π-Conjugated Molecular Films by Stepwise "Click" Assembly of Molecular Building Blocks: Characterizing Reaction Yield, Surface Coverage, and Film Thickness versus Addition Step Number

Abel T. Demissie,[†] Greg Haugstad,[‡] and C. Daniel Frisbie*[,†]

[†]Department of Chemical Engineering and Materials Science, University of Minnesota, 421 Washington Avenue SE, Minneapolis, Minnesota 55455, United States

[‡]Characterization Facility, University of Minnesota,100 Union Street SE, Minneapolis, Minnesota 55455, United States

Supporting Information

ABSTRACT: We report the systematic characterization of anisotropic, π-conjugated oligophenyleneimine (OPI) films synthesized using stepwise imine condensation, or "click" chemistry. Film synthesis began with a self-assembled monolayer (SAM) of 4-formylthiophenol or 4-aminothiophenol on Au, followed by repetitive, alternate addition of terephthalaldehyde (benzene-1,4-dicarbaldehyde) or 1,4-benzenediamine to form π-conjugated films ranging from 0.6−5.5 nm in thickness. By systematically capping the OPI films with a redox or halogen label, we were able to measure the relative surface coverage after each monomer addition via Rutherford backscattering spectrometry, X-ray photoelectron spectroscopy, spectroscopic ellipsometry, reflection−absorption infrared spectroscopy, and cyclic voltammetry. Nuclear reaction analysis was also employed for the first time on a SAM to calculate the surface coverage of carbon atoms after each stepwise addition. These six different analysis methods indicate that the average extent of reaction is 99% for each addition step. The high yield and molecular surface coverage confirm the efficacy of Schiff base chemistry, at least with the terephthalaldehyde and 1,4-benzenediamine monomers, for preparing high-quality molecular films with π conjugation normal to the substrate.

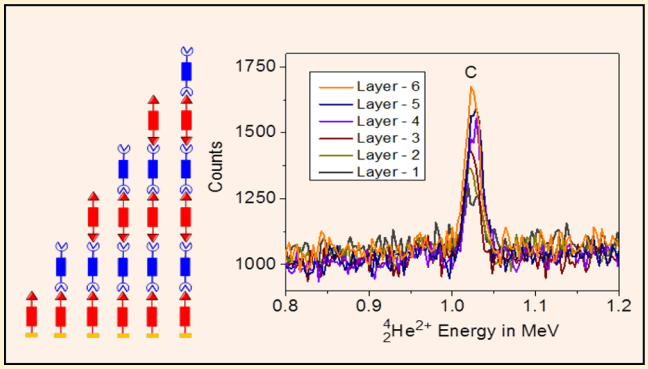

INTRODUCTION

Functional organic thin films with precisely tailored electronic and optical properties can be prepared using a variety of controlled stepwise monomer addition techniques. Marks and co-workers, for example, have prepared dielectric thin films for flexible electronics applications via siloxane-mediated stepwise reactions.[1−3] Others have employed metal ion coordination chemistry to build oriented organometallic films for molecular electronics experiments.[4] In our previous work, we have utilized Schiff base (imine) chemistry to assemble oriented, π-conjugated organic films from simple diamine- and dialdehyde-substituted building blocks.[5−8] Alternatively, we have employed the well-known azide−alkyne reaction chemistry to make π-conjugated films.[9] Each of these approaches relies on efficient "click" or "clicklike" reactions to ensure high reaction yields in a simple, sequential monomer addition process. Furthermore, click chemistry is self-limiting, much like atomic layer deposition (ALD) chemistry, so that one has precise nanometer-level control over the film architecture perpendicular to the substrate.

Film growth by imine click (condensation) chemistry is particularly useful for molecular electronics experiments because it provides a convenient means to obtain extended π conjugation in the growth direction. However, in the context of film growth from a solid substrate, the reaction yield per step has not been characterized previously, though it is obviously critically important. Low reaction yields—or even not very low yields, on the order of 90%—give rise to substantial and undesirable polydispersity in the molecular lengths normal to the substrate.

Here we have employed a battery of methods, including spectroscopic ellipsometry (SE), reflection−absorption infrared spectroscopy (RAIRS), Rutherford backscattering spectrometry (RBS), nuclear reaction analysis (NRA), X-ray photoelectron spectroscopy (XPS), and cyclic voltammetry (CV), to characterize the condensation reaction efficiency. To our knowledge, detailed characterization of stepwise-grown conjugated molecular wire films has not been reported previously. Furthermore, we have found new optimized conditions for growing the OPI wires that were not employed in our earlier work.[5] The characterization experiments are challenging

Received: April 30, 2015
Published: June 22, 2015

DOI: 10.1021/jacs.5b04512
J. Am. Chem. Soc. 2015, 137, 8819−8828

because the films are extremely thin. Indeed, we have found that our samples are an excellent platform for comparing a variety of surface analysis methods. A particularly unique aspect of this work is the use of NRA, which has not been employed before for analysis of self-assembled monolayers (SAMs) or ultrathin organic layers. Most importantly, we have found that, within error for all of the techniques we employed, these oligoimine condensation steps proceed essentially quantitatively and thus produce films of oriented π-conjugated molecules with low polydispersities, which is advantageous for the continued application of these systems in ongoing molecular electronics experiments.[10−25]

EXPERIMENTAL METHODS

Materials. Au nuggets were purchased from Mowrey Inc. (St. Paul, MN). Silicon wafers were purchased from Wafer Net (San Jose, CA). 4-Chlorothiophenol and aminoferrocene were purchased from TCI America (Portland, OR). Tetrabutylammonium hexafluorophosphate, 4-aminothiophenol (4-ATP), 1,4-benzenediamine, terephthalaldehyde, 4-iodobenzaldehyde, 4-iodoaniline, 4-chlorobenzaldehyde, 4-chloroaniline, 4-fluorobenzaldehyde, and 4-fluoroaniline were purchased from Sigma-Aldrich (St. Louis, MO). Absolute ethanol was purchased from Decon Laboratories (King of Prussia, PA). Dimethyl sulfoxide (DMSO) was purchased from Fisher Scientific (Waltham, MA), and acetonitrile was purchased from ACROS Organics (Geel, Belgium). 4-Formylthiophenol (4-FTP) was synthesized according to the literature.[26,27]

Wire Growth and Characterization. Au substrates were prepared using two different methods: conventional thermal evaporation and template stripping. For thermal evaporation, 50 Å of Cr was first evaporated on a bare Si wafer or mica as an adhesion layer, followed by 700 Å of Au, in a home-built evaporator at a rate of approximately 1−2 Å/s and a base pressure of $\lesssim 2 \times 10^{-6}$ Torr. For template-stripped Au (used only for XPS data shown in the Supporting Information), an epoxy adhesive was employed to bond small Si wafer pieces onto a 5000 Å thick Au film deposited by electron-beam evaporation on bare Si without any adhesion layer. The samples were then cured at approximately 150 °C for 1.5 h, and the Au layer was stripped off the bottom Si layer using a razor blade.

The Au substrates were then immersed into 1 mM 4-ATP (absolute ethanol) or 4-FTP (DMSO). After 24 h, the SAM-coated Au substrates were removed from the thiophenol solution, rinsed thoroughly with absolute ethanol to remove physisorbed molecules, and immersed into a 20 mM solution containing the next dialdehyde or diamine derivative depending on the wire design. Thus, the lengths of the wires were precisely controlled by alternate addition of the amine and aldehyde derivatives. In order to optimize the wire growth, aldehyde-terminated wires were reacted at 40 ± 2 °C with 1,4-benzenediamine for 24 h, and amine-terminated wires were reacted at room temperature (22 °C) with terephthalaldehyde for 24 h. As shown in Figure S1 in the Supporting Information, room-temperature reaction of aldehyde-capped wires with 1,4-benzenediamine resulted in incomplete disappearance of aldehyde peaks in the RAIRS spectra. Oligophenyleneimine (OPI) wires were kept in absolute ethanol before any surface characterization. Upon removal, the samples were rinsed again with absolute ethanol and blown dry with N_2 or Ar. The ferrocene capping reaction was carried out in a glovebox with <0.1 ppm of O_2 because aminoferrocene decomposes in air. The aldehyde-terminated wires were reacted with 2 mM aminoferrocene in absolute ethanol for a period of 24 h at room temperature. The samples were then rinsed, dried, and transferred to a clean centrifuge tube containing absolute ethanol before they were taken out of the glovebox for further rinsing (ethanol) and characterization.

RAIRS spectra were collected with a Nicolet iS50 spectrometer with a Harrick Seagull accessory for grazing-angle specular reflectance measurements. The incident angle for the p-polarized IR beam was 84° from the surface normal. For each sample and background, an average of 300 scans at a resolution of 2 cm^{-1} were collected after 15 min of purging with dry air.

Ellipsometry measurements were accomplished on a variable-angle spectroscopic ellipsometer (J. A. Woolam Co., Inc.). The change in polarization angles (ψ and Δ) were measured as a function of wavelength (λ) over the range of 600−1000 nm at incident angles of 55°, 65°, and 75°. To obtain accurate measurements, the background for each sample was measured before any wire growth to fit for Cr and Au thickness. Measurements of the polarization angles were performed again after completion of wire growth at the same position and incident angles as the background. The new ψ and Δ values along with the measured background thickness were used to fit for the thickness of the monolayers for fixed values of the index of refraction (n = 1.45) and the absorption coefficient (k = 0). From prior UV−vis spectroscopy work, the absorption coefficient for OPI wires was estimated to be approximately zero over the wavelength range of 600−1000 nm.[5]

XPS spectra were collected using an SSX-100-XPS system (Surface Science) equipped with a monochromatic Al Kα X-ray source (1486.3 eV) at a base pressure of $\lesssim 10^{-9}$ Torr. The Al X-ray anode was operated at 200 W, and the illuminated spot size on the sample was 0.64 mm^2. A hemispherical analyzer (at a 35° takeoff angle with respect to the sample normal) with constant pass energy was used to guide the photoemitted electrons toward the detector. The pass energy was 150 eV for survey scans and 50 eV for high-resolution scans. For each high-resolution scan, the binding energy was referenced to Au $4f_{7/2}$ (84.0 eV). The areas under the peaks of interest were fit using the Shirley background subtraction method, which removes the contribution of inelastically scattered electrons from the main peak.[28]

CV measurements were undertaken to measure the surface coverage of redox-capped wires with a Pine Instruments AFRDE5 potentiostat. A three-neck cylindrical electrochemical cell with a hole in the bottom was employed. An O-ring was placed between the bottom of the cell (0.9 cm in diameter) and the monolayer-coated Au substrate, which acted as the working electrode. The cell was then filled with 0.1 M tetrabutylammonium hexafluorophosphate, $[Bu_4N^+][PF_6^-]$, in extra-dry acetonitrile (<10 ppm H_2O). A Pt wire was employed as the counter electrode and a Ag wire as the quasi-reference electrode. The cell was purged with either N_2 or Ar gas prior to and during electrochemical measurements. For each monolayer, the scans were recorded at sweep rates of 100−500 mV/s, and the voltammograms were reproducible and stable to electrochemical cycling up to 1.2 V vs Ag wire.

Rutherford backscattering spectrometry was performed as a second measure of the surface coverage of monolayers capped with ferrocene. A MAS 1700 pelletron tandem ion accelerator (5SDH) equipped with a charge-exchange RF plasma source (National Electrostatics Corporation (NEC), Middleton, WI) was used to generate a 3.0 MeV $^4_2He^{2+}$ beam with a current of 30−40 nA measured at the sample. $^4_2He^{2+}$ ions backscattered by nuclear collisions (via Coulomb repulsion) were counted by an Ortec silicon ion detector that was positioned at a scattering angle of 165° with respect to the incident beam and subtended a solid angle of 3.6 msr. Spectra consisting of counts versus backscattered ion energy (with energetics described by classical billiard-ball kinematics) were acquired with a multichannel analyzer controlled by NEC RC43 software. The substrates were prepared by thermal evaporation of 20 nm of Au onto bare Si(100) without a Cr adhesion layer. Cr was not used because its backscattered peak lies close to the Fe peaks. The total integrated incident charge on the sample was Q = 100 μC per spectrum (40−60 min). The beam cross section was approximately 2 mm × 2 mm (square), but the sample was tilted by 75° (sample normal with respect to the beam) to improve the depth resolution, thereby elongating the analytical spot size to ∼8 mm along one dimension (the sample size was ∼15 mm along this dimension). Luminescent control samples of the same thickness were employed to precisely locate the beam position per sample goniometer coordinates. Quantitative comparisons between spectra (vertical scale) were achieved by normalization to the signal intensity of the Si substrate. This treatment accounted for small

DOI: 10.1021/jacs.5b04512
J. Am. Chem. Soc. 2015, 137, 8819−8828

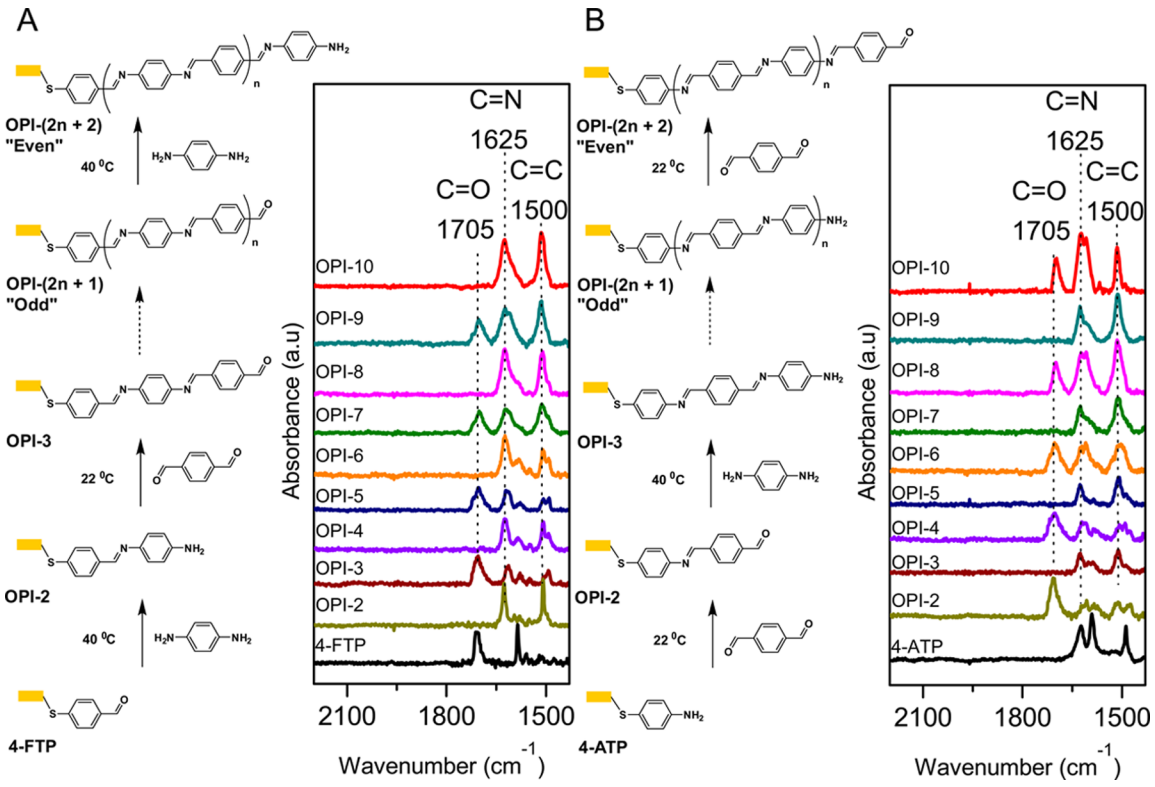

Figure 1. (A) Molecular structure and stepwise growth of OPI wires starting from 4-FTP (left) and corresponding RAIRS spectra (right) showing the alternate appearance and disappearance of aldehyde peaks. The aldehyde peaks appear for odd numbers of phenyl rings. (B) Molecular structure and stepwise growth of OPI wires starting from 4-ATP (left) and corresponding RAIRS spectra (right) showing the alternate appearance and disappearance of aldehyde peaks. The aldehyde peaks appear for even numbers of phenyl rings.

variations in the accuracy of beam current integration (i.e., error in the determination of Q).

For nuclear reaction analysis, the $^4_2He^{2+}$ ions were accelerated to 4.289 MeV in order to produce prompt nuclear reactions with carbon nuclei (described later) using a beam current of 30−40 nA at normal incidence (0° sample tilt and thus an analytical spot size of 2 mm × 2 mm). Backscattering $^4_2He^{2+}$ ions were detected as above but with a *strong enhancement in carbon sensitivity* due to a non-Rutherford nuclear-resonance scattering cross section[29] (i.e., with probability determined by nuclear quantum mechanics rather than classical Coulomb repulsion), while the energetics were still described by classical billiard-ball kinematics (i.e., elastic collisions) as in conventional RBS. The NRA substrates were prepared by thermal evaporation of 5 nm of Cr followed by 50 nm of Au on mica.

RESULTS AND DISCUSSION

Verification of Wire Growth and Length. OPI wires were prepared on Au surfaces by imine condensation click chemistry with alternating addition of terephthalaldehyde and 1,4-benzenediamine. In the notation OPI-*X*-*Y*, *X* represents the number of phenyl rings, and Y represents either a halogen (I) or ferrocene (Fc) capping unit (if present). Figure 1a,b displays the RAIRS spectra of OPI wires grown from SAMs of 4-FTP and 4-ATP, respectively, under the optimized conditions. Wires capped with carbonyl units appear at odd positions (OPI-3, OPI-5, OPI-7, and OPI-9) for wires grown from 4-FTP (Figure 1a) and at even positions (OPI-2, OPI-4, OPI-6, OPI-8, and OPI-10) for wires grown from 4-ATP (Figure 1b). The alternating appearance and disappearance of carbonyl stretch peaks[30] (1705 cm^{-1}) suggests an extent of reaction near completion for each step. The intensities of the imine stretch mode (C═N, 1625 cm^{-1})[30,31] and benzene ring stretch mode (C═C, 1500 cm^{-1})[30] increased with the number of repeat units, as expected. The sample dimensions for all of the RAIRS spectra were kept the same, allowing quantitative information about the extent of reaction to be reliably extracted from the carbonyl peak.

The extent of reaction for the nth click step as determined by FTIR was calculated from the carbonyl peak area ratio of OPI-n to OPI-$(n-1)$. The method assumes that the orientation of carbonyl peaks with respect to the p plane of the IR light electric field is the same for wires of different lengths. It should be noted that baseline correction of the spectra could easily introduce errors in the peak areas. As shown later (see Figure 8), the obtained results are scattered around a mean value of 98 ± 7.9%. This value does not deviate significantly from those obtained using other quantitative characterization methods, as will become clear below.

Ellipsometry was employed to determine the thicknesses of the wire films. As shown in Figure 2, the length of the wires increased with the number of repeat units. The estimated (theoretical) thickness was calculated by assuming a perpendicular orientation and trans configuration for each chain length. The index of refraction (n) and absorption coefficient (k) for ellipsometry were assumed to be 1.45 and 0, respectively, over the wavelength range of 600−1000 nm. The ellipsometry data are reasonably well matched to theoretical expectations. It is clear that films of up to 5.5 nm in thickness were synthesized. Comparison of the measured thicknesses with the theoretical predictions suggests an average tilt angle of 30° with respect to the surface normal.

Wire Surface Coverage As Determined by Cyclic Voltammetry. CV measurements were employed to calculate

DOI: 10.1021/jacs.5b04512
J. Am. Chem. Soc. 2015, 137, 8819−8828

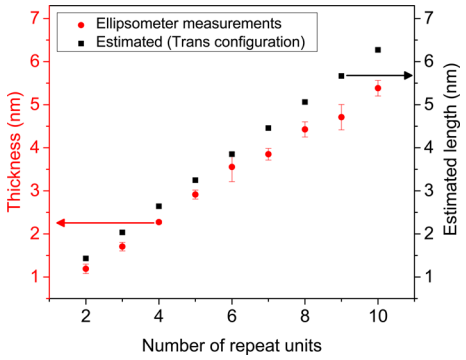

Figure 2. Measured and estimated thicknesses of OPI films as functions of the number of repeat units. The estimated thicknesses were calculated using Cambridge Scientific ChemBio 3D assuming a trans configuration of the molecules oriented normal to the substrate; the Au−S bond length was taken to be 2.36 Å.[5,46] The tilt angle was calculated from the inverse cosine of the ratio of the ellipsometer value to the theoretical prediction. Error bars represent one standard deviation.

the surface coverage and extent of reaction for OPI wires capped with redox-active ferrocene. As shown in Figure 3a, aldehyde-terminated OPI wires were reacted with amino-ferrocene to yield OPI-*X*-Fc wires. For each monolayer, CVs were recorded at sweep rates of 100, 200, 300, 400, and 500 mV/s and displayed reversible redox peaks characteristic of ferrocene.

For each wire length, at least three scans were averaged for each sweep rate on three different samples. Representative cyclic voltammograms for OPI-5-Fc at various sweep rates are shown in Figure 3b (CV data for other wires are plotted in Figure S2 in the Supporting Information). The cyclic voltammograms for all of the OPI-*X*-Fc wires exhibit a linear dependence on the sweep rate and excellent reversibility. Previous work by others has shown that electron transfer from Fc to metals through conjugated bridges can be very fast, though to our knowledge the OPI bridges reported here are longer than the oligophenylenevinylene (OPV) and oligophenyleneethynylene (OPE) bridges probed previously.[32,33] A detailed examination of the electron transfer kinetics will be the subject of a future study. We focus here on the surface analytical aspects, namely that the Fc coverage is reasonably constant for all wire lengths.

The surface coverage (N_s, in molecules/cm^2) for Fc centers was calculated according to eq 1:

$$N_s = \frac{Q}{nFA} \tag{1}$$

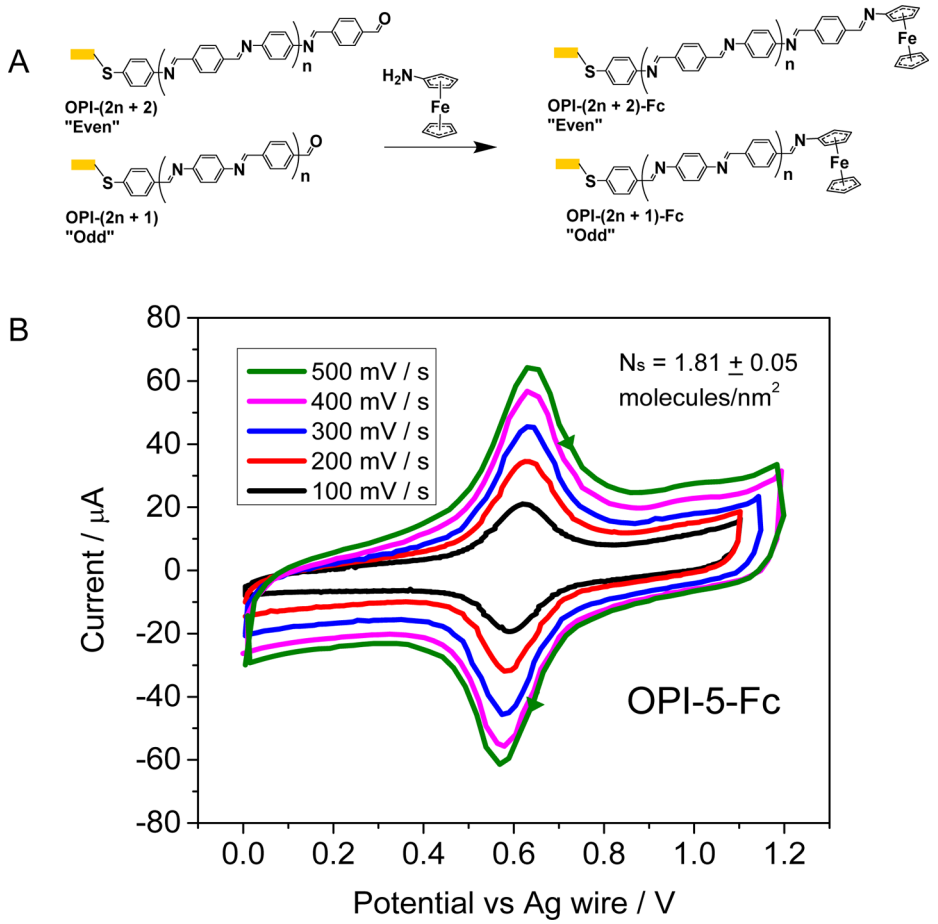

Figure 3. (A) Molecular structures of aldehyde-terminated wires on Au (left) before and (right) after capping with aminoferrocene. (B) Cyclic voltammograms of OPI-5-Fc at different sweep rates. The electrolyte was 0.1 M $[Bu_4N^+][PF_6^-]$ in acetonitrile. The reference and counter electrodes were Ag and Pt wires, respectively. The peak currents and sweep rates are linearly proportional, as expected for surface-confined species. Au geometrical area: 0.64 cm^2. Coverage of OPI-5-Fc: 1.81 ± 0.05 molecules/nm^2 (calculated from 200−500 mV/s sweep rates).

DOI: 10.1021/jacs.5b04512
J. Am. Chem. Soc. 2015, 137, 8819−8828

where Q is the charge injected into the SAM, n is the number of electrons involved in the transfer process (1), F is the Faraday constant, and A is the surface area of the monolayers examined (0.64 cm^2). The surface coverage results are plotted in Figure 4

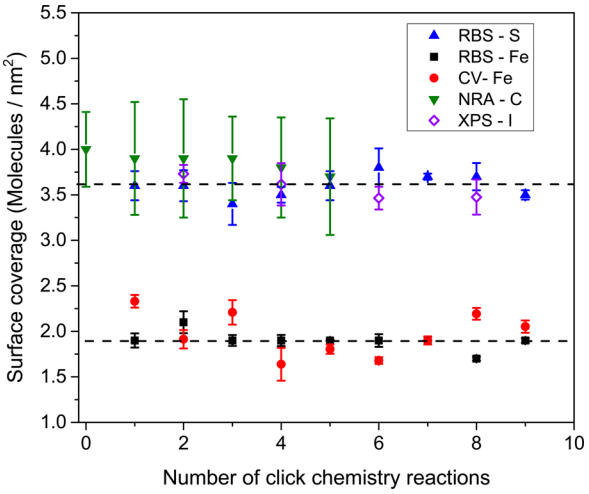

Figure 4. Surface coverage results obtained by RBS, CV, NRA, and XPS as functions of the number of click chemistry reactions (wire length). Blue triangles and black squares correspond to coverage values of S and Fe, respectively, from RBS, and red circles correspond to coverage values of Fe from CV. Inverted green triangles correspond to surface coverages of C atoms from NRA divided by the anticipated number of C atoms per wire, and violet diamonds correspond to surface coverages of I atoms from XPS. Error bars represent one standard deviation.

(red circles). The standard deviations derive from data sets of 60 sweeps for OPI-3-Fc to OPI-9-Fc and 30 sweeps for OPI-1-Fc and OPI-2-Fc. On average, the surface coverage of ferrocene-capped wires was 1.97 ± 0.24 molecules/nm^2. This value compares favorably with the coverages obtained for ferrocene-terminated alkylthiol SAMs on Au (typically 2.28–2.71 molecules/nm^2).[34,35]

Wire Surface Coverage As Determined by RBS. RBS is a nondestructive ion beam analysis technique that is used to measure elemental composition and, in suitable situations, its depth dependence. (Here we integrated signals from all depths of the thin organic films.) A beam of high energy $^4_2He^{2+}$ ions impinges on the sample, and the backscattered ion count versus energy spectrum is used to determine the elemental composition. The elemental surface coverage N_s (in atoms/cm^2) can also be determined by the following formula:[36]

$$N_s = \frac{A \cos\theta}{\left(\frac{d\sigma}{d\Omega}\right)\Omega Q} \quad (2)$$

where A is the total number of ions detected, θ is the tilt angle of the sample relative to the ion beam (75°), $d\sigma/d\Omega$ is the differential scattering cross section per unit solid angle (1.48×10^{-25} cm^2/sr for S or 3.99×10^{-25} cm^2/sr for Fe), Ω is the detector solid angle (3.6×10^{-3} sr), and Q is the total number of incident ions (3.0×10^{14}). There are only a few papers that have reported the use of RBS as a quantitative tool for organic monolayers.[37−39]

Figure 5b displays the RBS spectrum of OPI-9-Fc on thin Au (20 nm). The Au thickness was kept to 20 nm (not thicker) to ensure that the Fe peak would be clearly resolved from the

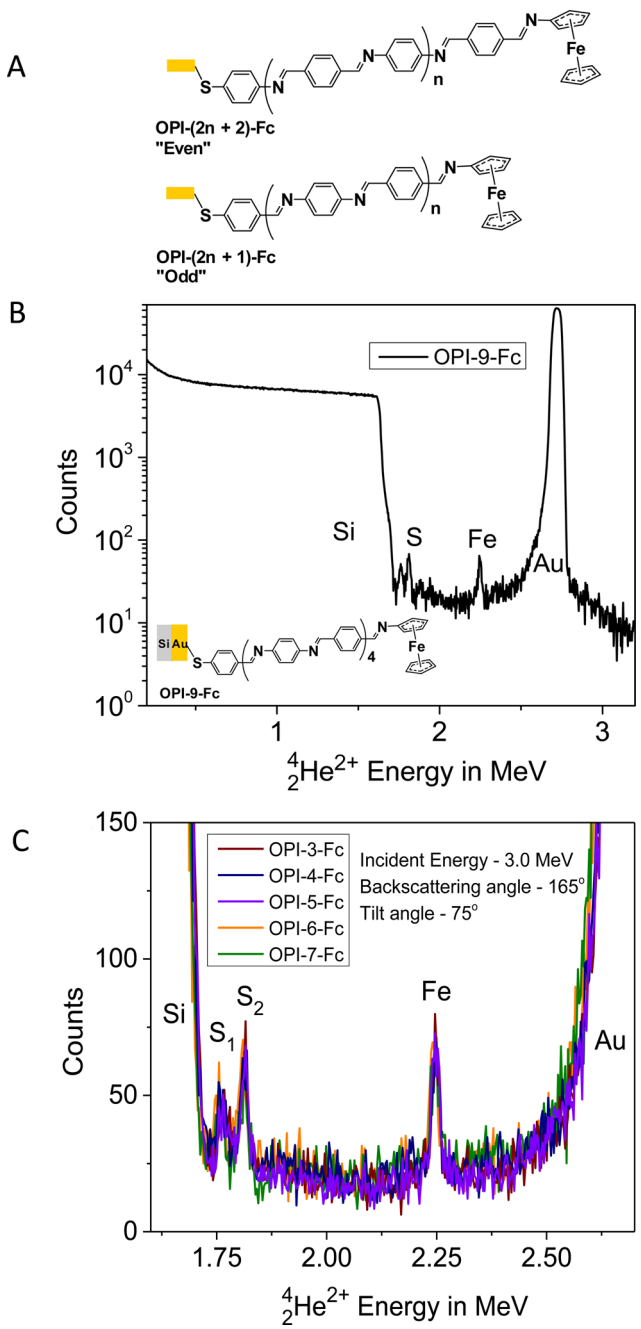

Figure 5. (A) Molecular structures of ferrocene (Fc)-terminated OPI wires. (B) RBS spectrum of OPI-9-Fc on a 20 nm Au film coated on Si without an adhesion layer. The S and Fe peaks are separated from the Si and Au signals. (C) RBS spectra of OPI-3-Fc, OPI-4-Fc, OPI-5-Fc, OPI-6-Fc, and OPI-7-Fc showing the S and Fe peaks. The spectral heights were normalized to the Si signal intensity.

broader Au peak. Clear signals were detected for S and Fe, as expected; a magnified view of the S and Fe region is shown in Figure 5c. Spectra were acquired with the incident beam impinging at an angle of 75° with respect to the sample normal at an energy of 3.0 MeV and at a backscattering angle of 165°. Tilting increases the energy loss of $^4_2He^{2+}$ ions that backscatter from a finite depth in the sample,[36] in our case resulting in separation of the S signals from two distinct depth locations.

To illustrate this point, the magnified spectra of OPI-3-Fc, OPI-4-Fc, OPI-5-Fc, OPI-6-Fc, and OPI-7-Fc are shown in Figure 5c (RBS spectra of other wires are plotted in Figure S5

DOI: 10.1021/jacs.5b04512
J. Am. Chem. Soc. 2015, 137, 8819−8828

in the Supporting Information). Three distinct peaks lie between the Si and Au signals, which are assigned to two S peaks and one Fe peak. Simulation of the RBS spectra with QUARK freeware indicated only the higher-energy sulfur peak, S_2, when the presence of S was modeled only at the film−Au interface. The lower-energy sulfur peak, S_1, could be simulated by incorporating roughly a monolayer of S at the Au−Si interface. Control spectra taken at other tilt angles and other beam energies were consistent with this assignment. No other simulated elemental assignments could reproduce the spectral peak locations.

The presence of "deep sulfur" (S_1) implicit in the preceding spectral analysis suggests diffusion of the 4-ATP or 4-FTP molecules to the Au−Si interface via the Au grain boundaries during the first chemisorption step. To test our hypothesis, we prepared 20 and 40 nm Au substrates and flame-annealed them before adsorption of 4-ATP. The purpose of annealing was to increase the grain size of the Au and reduce the total number of grain boundaries. If the 4-ATP or 4-FTP molecules diffused via grain boundaries, then reducing the number of grain boundaries should reduce the number of molecules reaching the Au−Si interface. The results shown in Figure S4 in the Supporting Information were consistent with our hypothesis: only one S peak (S_2) was detected. Furthermore, the unannealed 40 nm Au substrate also showed no S_1 peaks, supporting our conclusion because thicker Au layers present a greater diffusion barrier. However, we decided to collect the final RBS spectra (Figure 5) using 20 nm unannealed Au films because annealing results in greater tailing of the Au peak edge toward the Fe peak due to an increase in Au surface roughness (grain coarsening).

The surface coverages of OPI-*X*-Fc wires were calculated according to eq 2. The areas under the S_2 and Fe peaks were integrated to yield the total numbers of ions backscattered from the S and Fe units. The differential scattering cross sections were calculated from the equation of Marion and Young.[36] For each sample, two distinct locations were analyzed, and the results are plotted in Figure 4. On average, we obtained surface coverage values of 1.9 ± 0.1 and 3.6 ± 0.1 molecules/nm^2 for Fe and S, respectively.

Our results indicate that on average only 52% (1.9/3.6) of the wires were capped with ferrocene. This was also confirmed by the IR spectra in Figure S6 in the Supporting Information, which showed unreacted carbonyl peaks after the capping reaction with aminoferrocene. In fact, the ratio of the carbonyl peak area of OPI-3-Fc to that of OPI-3 gave a value of 38%, indicating that only 62% of OPI-3 wires were capped with ferrocene. To further investigate whether this was due to reaction kinetics or steric effects, the RBS spectrum of 6-(ferrocenyl)hexanethiol (Figure S7 in the Supporting Information) was compared to those of the OPI-*X*-Fc wires. The surface coverage values for 6-(ferrocenyl)hexanethiol were 2.1 and 2.1 molecules/nm^2 for S and Fe, respectively, very similar to the ferrocene coverage values obtained by both CV and RBS for OPI-*X*-Fc wires. We believe that it is not energetically favorable to pack more than two ferrocene molecules per square nanometer and that steric effects are likely the reason that aminoferrocene did not react completely with the carbonyl units on the OPI wires. Collectively, the RBS data give us a quantitative coverage measurement that is consistent with the cyclic voltammetry results. Figure 4 suggests that the wire coverage is ∼3.6 OPI wires/nm^2.

Wire Surface Coverage As Determined by NRA. Our ion beam analysis instrument at Minnesota also provides for quantitative nuclear reaction analysis of low-atomic-mass elements, such as C, that are difficult to detect with RBS because their signals lie spectrally atop the much stronger substrate signal (as the Rutherford backscattering peak counts are proportional to the square of the atomic number) with its correspondingly substantial noise. In NRA, an incident $^4_2He^{2+}$ ion may initiate a nuclear reaction by penetrating a target nucleus if it has enough energy to overcome the Coulomb barrier, forming an intermediate excited nuclear state that immediately decays back to the ground state by emission of a particle in the case of *prompt* reactions. (Some nuclear reactions generate radioactive states that decay more slowly, on the scale of minutes to hours, but we did not access such reactions in the present work.) This non-Rutherford scattering process can result in a distinct enhancement of the signal (peak intensity) of target nuclei because the quantum mechanics for activation of such nuclear states produces a scattering cross section that is much greater than that of Rutherford (classical Columbic) scattering. For $^1_1H^+$ and $^4_2He^{2+}$ projectiles with incident energies up to at most a few MeV (as are accessible with small accelerators in materials characterization facilities), there are only a few elements such as C, N, and O with analytically useful nuclear cross sections.[40] Thus, NRA cannot be used for the detection of arbitrary elements; rather, here we exploited the known reaction of $^{12}_6C$ with $^4_2He^{2+}$ at 4.289 MeV to measure the carbon coverage.

When the energy of the incident α particles is increased to 4.289 MeV, the nuclear reaction between $^{12}_6C$ and $^4_2He^{2+}$ forms an unstable $^{16}_8O^{2+}$ intermediate that immediately decays back to $^{12}_6C$ and $^4_2He^{2+}$ (as shown in eq 3), with the energetics of

$$^{12}_6C + {}^4_2He^{2+}(4.289\ \text{MeV}) \rightarrow {}^{16}_8O^{2+} \rightarrow {}^{12}_6C + {}^4_2He^{2+}(1.022\ \text{MeV}) \quad (3)$$

scattering, and thus the spectral peak position, being identical to those in the Rutherford case. As with conventional RBS, the emitted $^4_2He^{2+}$ particles can then be counted to yield the surface coverage of C atoms following calibration to the enhanced nuclear scattering cross section. To our knowledge, this is the first work that has utilized NRA as a characterization tool for SAMs.

The OPI wires for NRA were synthesized starting from a SAM of 4-ATP followed by alternating addition of terephthalaldehyde or 1,4-benzenediamine in the usual manner. In order to reduce channeling in the substrate (as happens for the case of an untilted Si(100) substrate, reducing its signal) and thereby retain the utility of the substrate signal intensity for spectral normalization, mica substrates with 5 nm of Cr and 50 nm of Au (deposited by thermal evaporation) were employed. As shown in Figure 6a, wires with even numbers of phenyl rings (OPI-2, OPI-4, and OPI-6) were capped with benzaldehyde, and wires with odd numbers of phenyl rings (OPI-3 and OPI-5) were capped with 1,4-benzenediamine. The NRA C spectra in Figure 6b show a linear relationship between the intensity of carbon counts and the total number of repeat units, i.e., each stepwise addition resulted in an increase in the integrated number of $^4_2He^{2+}$ ions scattered from $^{12}_6C$ nuclei, as expected. The surface coverage was calculated from eq 2 (similar to RBS of OPI-*X*-Fc wires), and the nuclear scattering cross section was interpolated from a table by Feng et al.[29] to be ((5.195 ± 0.103) × 10^{-25} cm^2/sr). The total number of incident particles was 1.5 × 10^{14}.

DOI: 10.1021/jacs.5b04512
J. Am. Chem. Soc. 2015, 137, 8819−8828

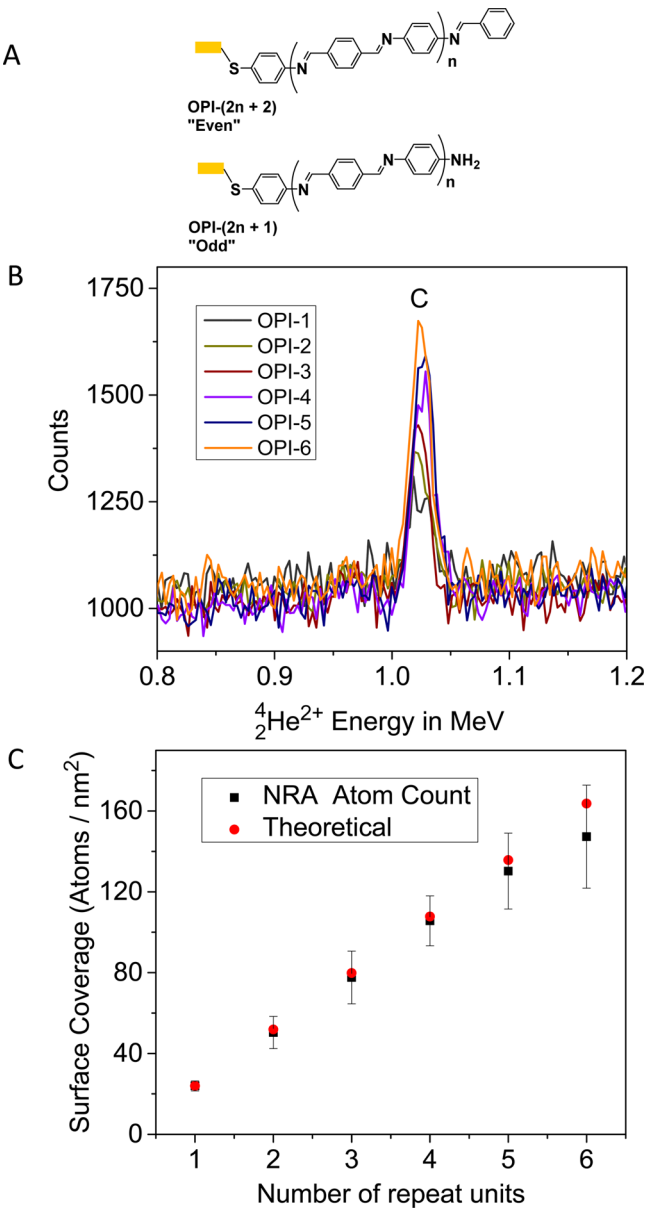

Figure 6. (A) Molecular structures of OPI wires capped with benzaldehyde (even positions) and uncapped (odd positions) for NRA. (B) NRA C spectra of OPI-1, OPI-2, OPI-4, OPI-5, and OPI-6 wires. Each stepwise addition resulted in an increase in the C peak intensity. The spectral heights were normalized to the substrate signal. (C) Surface coverage values for C atoms (black squares) as a function of number of repeat units. The error bars represent one standard deviation.

The C surface coverage values are shown in Figure 6c for the first six repeat units (two scans per sample). In order to correct for adventitious adsorbed hydrocarbons from the chamber, the *y*-intercept from a linear fit to a plot of raw peak area versus number of repeat units was subtracted. The approximate linear growth in the C concentration is excellent evidence that the wire synthesis proceeds as outlined in Figure 1 and our previous papers,[5,6] and it is consistent with the thickness data in Figure 2. The molecule count, as shown in Figure 4, was obtained by dividing the atom count by the expected number of carbon atoms per chain. On average, we obtained a surface coverage value of 3.9 ± 0.1 molecules/nm^2 for C, which is in excellent agreement with values obtained for S using RBS (Figure 4).

Wire Surface Coverage As Determined by XPS. The availability of para-halogenated anilines or benzaldehydes from commercial sources makes these species ideal tags to investigate OPI wire synthesis by XPS. Among all of the halogenated anilines or benzaldehydes, iodine is the best XPS tag because it has the highest photoemission cross section (8.39×10^{-23} m^2), followed by bromine (1.35×10^{-23} m^2), fluorine (6.36×10^{-24} m^2), and chlorine (5.86×10^{-24} m^2).[41] Thus, spectra with good signal-to-noise ratio could be obtained with acquisition times of 30 min for I tags versus 240 min for Cl tags. For F-labeled monomers, the coverage was anomalously low, presumably because the electron-withdrawing F substituent decreased the reactivity of 4-fluoroaniline with the formyl units.

OPI wires were capped with I by reacting the aldehyde termini with 4-iodoaniline, as shown in Figure 7a. The spectra in Figure 7b show photoemission counts for I 3d peaks, and the two pairs of peaks correspond to different chemical states of I. To rule out any contribution from charging effects on the substrate, the spectrum of OPI-3-I was collected by applying an electron neutralizer. The results shown in Figure S11 in the Supporting Information indicate that both peaks were present up to neutralizer energies of 10 eV and thus likely represent two different chemical states. Iodine is known to bind to coinage metals such as Cu, Ag, and Au.[42] To determine which pairs of peaks are from the iodophenylene units (wires) and which are from Au−I bonds, a blank Au substrate was inserted into a 20 mM solution of 4-iodobenzaldehyde. The spectrum in Figure S12 in the Supporting Information clearly shows that only the β peaks were present for the blank Au substrate, which indicates that the α peaks observed for OPI samples correspond to C−I bonds, which are the peaks of interest for calculating the surface coverage.

The surface coverage of I ($N_{s(I)}$) was calculated according to eq 4:

$$N_{s(I3d_{5/2})} = \frac{\Gamma_{I3d_{5/2}}\sigma_{Au4p_{3/2}}Q_{Au4p_{3/2}}L_{Au4p_{3/2}}\rho_{Au}\lambda_{Au}t_{Au4p_{3/2}}\cos\theta}{\Gamma_{Au4p_{3/2}}\sigma_{I3d_{5/2}}L_{I3d_{5/2}}t_{I3d_{5/2}}} \quad (4)$$

where Γ is the peak area, t is the scan time, σ is the photoionization cross section[41] ($\sigma_{Au4p_{3/2}} = 8.01 \times 10^{-24}$ m^2 and $\sigma_{I3d_{5/2}} = 2.70 \times 10^{-23}$ m^2), Q is the correction term for elastic scattering[28] ($Q_{Au4p_{3/2}} = 0.92$), L is a function of the angular asymmetry factor β (which describes the anisotropy of photoemission[28,43]) and the angle ψ between the X-ray and the analyzer (71°) ($L_{Au4p_{3/2}} = 0.0913$, $L_{I3d_{5/2}} = 0.0954$), ρ_{Au} is the atomic density of Au (59.04 atoms/nm^3), λ is the inelastic photoelectron mean free path[28,44] ($\lambda_{Au} = 2.23$ nm), f is the fraction of photoelectrons that appear in the main peak[45] ($f_{Au} = f_I = 0.84$), and θ is the takeoff angle measured with respect to the sample normal ($\theta = 35°$). A detailed derivation of eq 4 and low-resolution spectra of OPI-*X*-I wires are available in the Supporting Information (Figure S13). At low resolution (typically used in survey scans), the transmission function can be assumed to be constant for photoelectrons of similar kinetic energy, such as Au $4p_{3/2}$ (KE = 940 eV) and I $3d_{5/2}$ (KE = 866 eV). This approximation does not hold for high-resolution spectra, where the transmission function is not linearly related to the kinetic energy. Thus, we were not able to convert the peak area values to surface coverages for the high-resolution

DOI: 10.1021/jacs.5b04512
J. Am. Chem. Soc. 2015, 137, 8819−8828

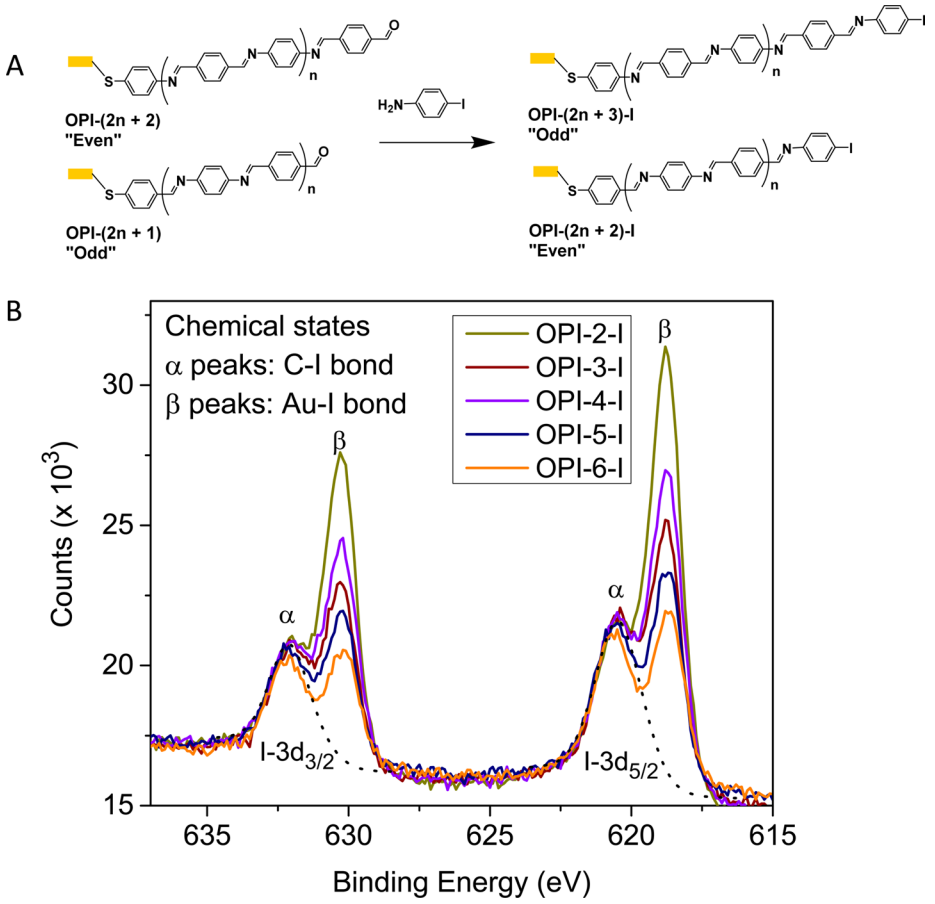

Figure 7. (A) Molecular structures of aldehyde-terminated wires (left) before and (right) after capping with 4-iodoaniline. (B) High-resolution I 3d XPS spectra for OPI-2-I, OPI-3-I, OPI-4-I, OPI-5-I, and OPI-6-I. The two pairs of peaks are from different chemical states of I. The α peaks are from C−I bonds, while the β peaks are from Au−I bonds. A detailed discussion of the peak assignment and peak stability is available in the Supporting Information.

spectra (Figure S14 in the Supporting Information).The α-I $3d_{5/2}$ surface coverage values obtained from low-resolution scans of OPI-3-I, OPI-5-I, OPI-7-I, and OPI-9-I are shown in Figure 4. At ~3.57 I tags/nm^2, they are in good agreement with the results obtained by RBS, CV, and NRA.

The high-resolution XPS spectra in Figure 7b were acquired at three different locations for each sample, and the averages of the I $3d_{5/2}$ and I $3d_{3/2}$ normalized peak areas were used for calculating the extent of reaction. All of the data were fit by using a combination of Lorentzian and Gaussian peak shapes such that the spin−orbit coupling rule was obeyed. In order to check the degradation of the sample under prolonged X-ray beam exposure, a series of high-resolution spectra for I-terminated wires were collected at the same position for up to 2.5 h. The results shown in Figure S14 indicate that α peaks were stable under exposure to the X-ray beam for up to 2 h and dropped only by 10% in absolute area afterward. Figure S16 in the Supporting Information displays the normalized peak areas for the α-I peaks as a function of the number repeat units. On average, within error, there is not much variation in the area of the α-I peak as a function of the number of repeat units. Thus, this is consistent with near-quantitative stepwise reaction.

Reaction Yield per Synthesis Step. A central goal of our work was to determine the reaction yield for the surface click reactions (Figure 8). This was achieved from the ratios of consecutive average surface coverage values obtained by RBS, CV, and NRA, carbonyl peak areas from IR, and iodine peak areas from XPS (eq 5):

$$\text{extent of reaction} = \frac{\text{signal due to } (\text{OPI})_n}{\text{signal due to } (\text{OPI})_{n-1}} \quad (5)$$

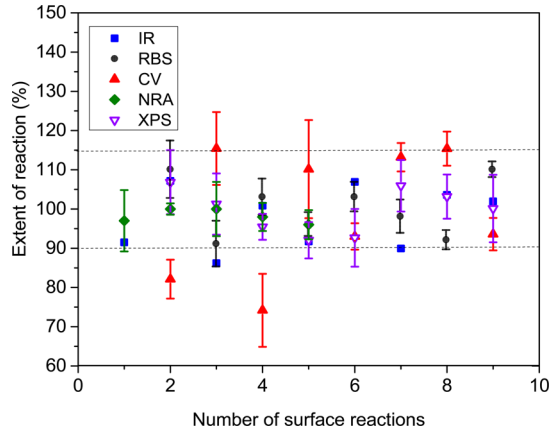

Figure 8. Extents of reaction of OPI wires obtained by different techniques as functions of the number of surface reactions. The results for CV, RBS, and NRA were obtained from surface coverage values (Figure 4), whereas the IR and XPS results were obtained from peak areas associated with carbonyl and iodine units, respectively.

DOI: 10.1021/jacs.5b04512
J. Am. Chem. Soc. 2015, 137, 8819−8828

For example, to calculate the extent of reaction for the fifth step by XPS, the ratio of the I peak area for OPI-5-I (19.1×10^3) to that for OPI-4-I (20.0×10^3) from Figure 7 was evaluated, giving a value of 96%. The extents of reaction measured by the different methods, as averages of the first nine surface reactions, yielded values of 98 ± 7.9% by FTIR, 99 ± 6.6% by RBS, 99 ± 16% by CV, 99 ± 5.8% by XPS, and 98 ± 2.4% by NRA. It is evident that these yields are remarkably similar across the five different techniques and the five different tags. Averaging across all of the techniques, we estimate the extent of reaction to be 99% per step.

The scatter evident in Figure 8 deserves some discussion. Fundamentally, quantitative surface analysis is challenging because of the low numbers of molecules/atoms per unit area. For example, typical XPS uncertainties for atomic concentrations are on the order of 5−10%. One can see that if the reaction yields are near-quantitative, then uncertainties can lead to reaction yield estimates for a single step that are greater than 100%. This might be better understood by inspection of the NRA data in Figure 6c. The quality of these data is quite high, but if it were worse (i.e., if there were more vertical scatter for each experimental point), then ratioing the coverages for consecutive steps (e.g., the coverage after four reactions divided by the coverage after three reactions) could easily give an apparent yield greater than 100%. The actual NRA estimate of the extent of reaction in Figure 8 is reasonably tight across consecutive surface reactions. These are our highest-quality data. In connection with Figure 8, it should be clear that we are not claiming that the reaction yield is ever over 100%. The percentages in Figure 8 represent the uncertainties of the measurements and the combination of errors when employing eq 5.

In a sense, Figure 4 is more meaningful than Figure 8. Figure 4 shows that within experimental error, the coverage of tag elements is unchanged for consecutive reactions.

It is also evident from Figure 8 that the extent of reaction varies as much as 40% for CV and approximately 10−20% for the other methods. This could be due to both the large scan size for CV (10× greater than for RBS and XPS), which makes it more prone to defects on Au, and contributions from the onset of an irreversible redox process in the OPI wires around 0.7 V.

Importantly, the chain length distribution can be calculated from the extent of reaction of each reaction step. Given the average yield per step of 99%, the chain length distribution is as shown in Figure S17b in the Supporting Information after nine click reactions. That is, for 10 repeat units, 91% of the chains will have the expected length. On the other hand, if the extent of reaction for each step were to proceed to 90% completion, the chain length distribution for the longest wire would decrease significantly to the point that only 38% of the wires would contain the wire length of interest after nine surface reactions, as shown in Figure S17a. This is important information for ongoing molecular electronics experiments that employ these wires.

■ CONCLUSION

We have systematically measured the coverage and surface reaction yield for a set of π-conjugated molecular wires ranging in length from 0.6 to 5.5 nm. The OPI wires were grown from SAMs of 4-aminothiophenol or 4-formylthiophenol and reacted stepwise with alternating addition of terephthalaldehyde (22 °C) or 1,4-benzenediamine (40 °C). Surface analysis by six different techniques (SE, CV, IR, RBS, NRA, and XPS) demonstrated that the surface reaction yields via imine click chemistry are high, approximately 99%. The high yields and correspondingly high surface coverages of π-conjugated molecular wires (3.5 molecules/nm^2) bode well for the continued use of these systems in ongoing molecular electronics experiments. Additionally, these OPI wires serve as an excellent platform for quantitative comparison of different surface analytical techniques and in particular for demonstrating the effective use of NRA for SAM characterization for the first time. Future work will focus on the synthesis of OPI wires with a broad spectrum of backbone architectures to enhance electronic functionality.

■ ASSOCIATED CONTENT

Supporting Information

Detailed experimental characterization and discussions of OPI-*X*-Fc, halogen-incorporated, and halogen-tagged OPI wires and the derivation of eq 4. The Supporting Information is available free of charge on the ACS Publications website at DOI: 10.1021/jacs.5b04512.

■ AUTHOR INFORMATION

Corresponding Author

*frisbie@umn.edu

Notes

The authors declare no competing financial interest.

■ ACKNOWLEDGMENTS

This project was supported primarily by NSF under Award CHE-1213876. Partial support came from the NSF MRSEC Program under Award DMR-0819885 and from the UMN Industrial Partnership for Research in Interfacial Materials & Engineering (IPRIME). Parts of this work were carried out in the Characterization Facility, University of Minnesota, which receives partial support from NSF through the MRSEC program.

■ REFERENCES

(1) Lin, W.; Lin, W.; Wong, G. K.; Marks, T. J. *J. Am. Chem. Soc.* **1996**, *118*, 8034.
(2) Yoon, M.-H.; Facchetti, A.; Marks, T. J. *Proc. Natl. Acad. Sci. U.S.A.* **2005**, *102*, 4678.
(3) DiBenedetto, S. A.; Facchetti, A.; Ratner, M. A.; Marks, T. J. *Adv. Mater.* **2009**, *21*, 1407.
(4) Tuccitto, N.; Ferri, V.; Cavazzini, M.; Quici, S.; Zhavnerko, G.; Licciardello, A.; Rampi, M. A. *Nat. Mater.* **2009**, *8*, 41.
(5) Choi, S. H.; Kim, B.; Frisbie, C. D. *Science* **2008**, *320*, 1482.
(6) Choi, S. H.; Frisbie, C. D. *J. Am. Chem. Soc.* **2010**, *132*, 16191.
(7) Luo, L.; Choi, S. H.; Frisbie, C. D. *Chem. Mater.* **2011**, *23*, 631.
(8) Luo, L.; Balhorn, L.; Vlaisavljevich, B.; Ma, D.; Gagliardi, L.; Frisbie, C. D. *J. Phys. Chem. C* **2014**, *118*, 26485.
(9) Luo, L.; Frisbie, C. D. *J. Am. Chem. Soc.* **2010**, *132*, 8854.
(10) Yuan, L.; Jiang, L.; Zhang, B.; Nijhuis, C. A. *Angew. Chem., Int. Ed.* **2014**, *53*, 3377.
(11) Cabarcos, O. M.; Shaporenko, A.; Weidner, T.; Uppili, S.; Dake, L. S.; Zharnikov, M.; Allara, D. L. *J. Phys. Chem. C* **2008**, *112*, 10842.
(12) Bonifas, A. P.; McCreery, R. L. *Nano Lett.* **2011**, *11*, 4725.
(13) Sangeeth, C. S. S.; Wan, A.; Nijhuis, C. A. *J. Am. Chem. Soc.* **2014**, *136*, 11134.
(14) Lavi, A.; Cohen, H.; Bendikov, T.; Vilan, A.; Cahen, D. *Phys. Chem. Chem. Phys.* **2011**, *13*, 1293.
(15) Nijhuis, C. A.; Reus, W. F.; Whitesides, G. M. *J. Am. Chem. Soc.* **2009**, *131*, 17814.

DOI: 10.1021/jacs.5b04512
J. Am. Chem. Soc. 2015, 137, 8819−8828

(16) Lewis, P. A.; Inman, C. E.; Maya, F.; Tour, J. M.; Hutchison, J. E.; Weiss, P. S. *J. Am. Chem. Soc.* **2005**, *127*, 17421.
(17) Aradhya, S. V.; Venkataraman, L. *Nat. Nanotechnol.* **2013**, *8*, 399.
(18) Vericat, C.; Vela, M. E.; Benitez, G.; Carro, P.; Salvarezza, R. C. *Chem. Soc. Rev.* **2010**, *39*, 1805.
(19) Hihath, J.; Tao, N. *Semicond. Sci. Technol.* **2014**, *29*, No. 054007.
(20) Heimel, G.; Zojer, E.; Romaner, L.; Brédas, J.-L.; Stellacci, F. *Nano Lett.* **2009**, *9*, 2559.
(21) Bergfield, J. P.; Ratner, M. A. *Phys. Status Solidi B* **2013**, *250*, 2249.
(22) Rosink, J. J. W. M.; Blauw, M. A.; Geerligs, L. J.; van der Drift, E.; Rousseeuw, B. A. C.; Radelaar, S.; Sloof, W. G.; Fakkeldij, E. J. M. *Langmuir* **2000**, *16*, 4547.
(23) Alloway, D. M.; Hofmann, M.; Smith, D. L.; Gruhn, N. E.; Graham, A. L.; Colorado, R.; Wysocki, V. H.; Lee, T. R.; Lee, P. A.; Armstrong, N. R. *J. Phys. Chem. B* **2003**, *107*, 11690.
(24) Willicut, R. J.; McCarley, R. L. *Langmuir* **1995**, *11*, 296.
(25) Bâldea, I.; Xie, Z.; Frisbie, C. D. *Nanoscale* **2015**, *7*, 10465.
(26) Golchoubian, H.; Hosseinpoor, F. *Molecules* **2007**, *12*, 304.
(27) Young, R. N.; Gauthier, J. Y.; Coombs, W. *Tetrahedron Lett.* **1984**, *25*, 1753.
(28) Powell, C. J.; Jablonski, A. *J. Electron Spectrosc. Relat. Phenom.* **2010**, *178*−*179*, 331.
(29) Feng, Y.; Zhou, Z.; Zhou, Y.; Zhao, G. *Nucl. Instrum. Methods Phys. Res., Sect. B* **1994**, *86*, 225.
(30) Lin-Vien, D.; Colthup, N. B.; Fateley, W. G.; Grasselli, J. G. *The Handbook of Infrared and Raman Characteristic Frequencies of Organic Molecules*; Academic Press: San Diego, CA, 1991.
(31) Ledbetter, J. W. *J. Phys. Chem.* **1977**, *81*, 54.
(32) Smalley, J. F.; Sachs, S. B.; Chidsey, C. E. D.; Dudek, S. P.; Sikes, H. D.; Creager, S. E.; Yu, C. J.; Feldberg, S. W.; Newton, M. D. *J. Am. Chem. Soc.* **2004**, *126*, 14620.
(33) Sikes, H. D.; Smalley, J. F.; Dudek, S. P.; Cook, A. R.; Newton, M. D.; Chidsey, C. E.; Feldberg, S. W. *Science* **2001**, *291*, 1519.
(34) Valincius, G.; Niaura, G.; Kazakeviciene, B.; Talaikyte, Z.; Kazemekaite, M.; Butkus, E.; Razumas, V. *Langmuir* **2004**, *20*, 6631.
(35) Walczak, M. M.; Popenoe, D. D.; Deinhammer, R. S.; Lamp, B. D.; Chung, C.; Porter, M. D. *Langmuir* **1991**, *7*, 2687.
(36) Chu, W.-K.; Mayer, J. W.; Nicolet, M. *Backscattering Spectrometry*; Academic Press: New York, 1978.
(37) Colvin, V. L.; Goldstein, A. N.; Alivisatos, A. P. *J. Am. Chem. Soc.* **1992**, *114*, 5221.
(38) Wohlfart, P.; Weiß, J.; Käshammer, J.; Winter, C.; Scheumann, V.; Fischer, R. A.; Mittler-Neher, S. *Thin Solid Films* **1999**, *340*, 274.
(39) Beebe, J. M.; Engelkes, V. B.; Liu, J.; Gooding, J. J.; Eggers, P. K.; Jun, Y.; Zhu, X.; Paddon-Row, M. N.; Frisbie, C. D. *J. Phys. Chem. B* **2005**, *109*, 5207.
(40) *Surface and Thin Film Analysis: A Compendium of Principles, Instrumentation and Applications*; Bubert, H., Jenett, H., Eds.; Wiley-VCH: Weinheim, Germany, 2002.
(41) Scofield, J. H. *J. Electron Spectrosc. Relat. Phenom.* **1976**, *8*, 129.
(42) Berry, G. M.; Bravo, B. G.; Bothwell, M. E.; Cali, G. J.; Harris, J. E.; Mebrahtu, T.; Michelhaugh, S. L.; Rodriguez, J. F.; Soriaga, M. P. *Langmuir* **1989**, *5*, 707.
(43) Reilman, R. F.; Msezane, A.; Manson, S. T. *J. Electron Spectrosc. Relat. Phenom.* **1976**, *8*, 389.
(44) Seah, M. P.; Gilmore, I. S. *Surf. Interface Anal.* **1998**, *26*, 908.
(45) Yarzhemsky, V. G.; Nefedov, V. I.; Trzhaskovskaya, M. B.; Band, I. M.; Szargan, R. *J. Electron Spectrosc. Relat. Phenom.* **2002**, *123*, 1.
(46) Tour, J. M.; Jones, L.; Pearson, D. L.; Lamba, J. J. S.; Burgin, T. P.; Whitesides, G. M.; Allara, D. L.; Parikh, A. N.; Atre, S. *J. Am. Chem. Soc.* **1995**, *117*, 9529.

DOI: 10.1021/jacs.5b04512
J. Am. Chem. Soc. 2015, 137, 8819−8828